

**Electronic Supplementary Material (ESI) for Catalysis Science &  
Technology**

Supporting Information for

**Dry reforming of methane over Co-Mo/Al<sub>2</sub>O<sub>3</sub> catalyst at low  
microwave power irradiation**

Hoang M Nguyen <sup>a</sup>, Gia Hung Pham<sup>a\*</sup>, Ran Ran<sup>a</sup>, Robert Vagnoni<sup>b</sup>, Vishnu Pareek<sup>a</sup>,  
Shaomin Liu<sup>a\*</sup>

<sup>a</sup>. Department of Chemical Engineering, Curtin University, GPO Box U1987, Perth,  
Western Australia, 6845, Australia.

<sup>b</sup>. Eco Technol Co., Pty Ltd, Perth, Western Australia, 6009, Australia.

*Corresponding authors:*

Emails:

G.Pham@curtin.edu.au (G.H.Pham)

Shaomin.Liu@curtin.edu.au (S. Liu)

## Experimental

**Table. S 1.** List of chemicals used in the study.

Name	Formula	Grade, %	Supplier
Cobalt (II) Nitrate	$\text{Co}(\text{NO}_3)_2 \cdot 6\text{H}_2\text{O}$	99	Chem. Supply
Ammonium Molybdate Tetrahydrate	$(\text{NH}_4)_6\text{Mo}_7\text{O}_{24} \cdot 4\text{H}_2\text{O}$	99	Chem. Supply
Quartz wool	-	99.3	Thermo Fisher Scientific
Aluminium Oxide	$\text{Al}_2\text{O}_3$	99	Sasol Germany GmbH
Ethanol	$\text{C}_2\text{H}_6\text{O}$	98.9	Chem. Supply

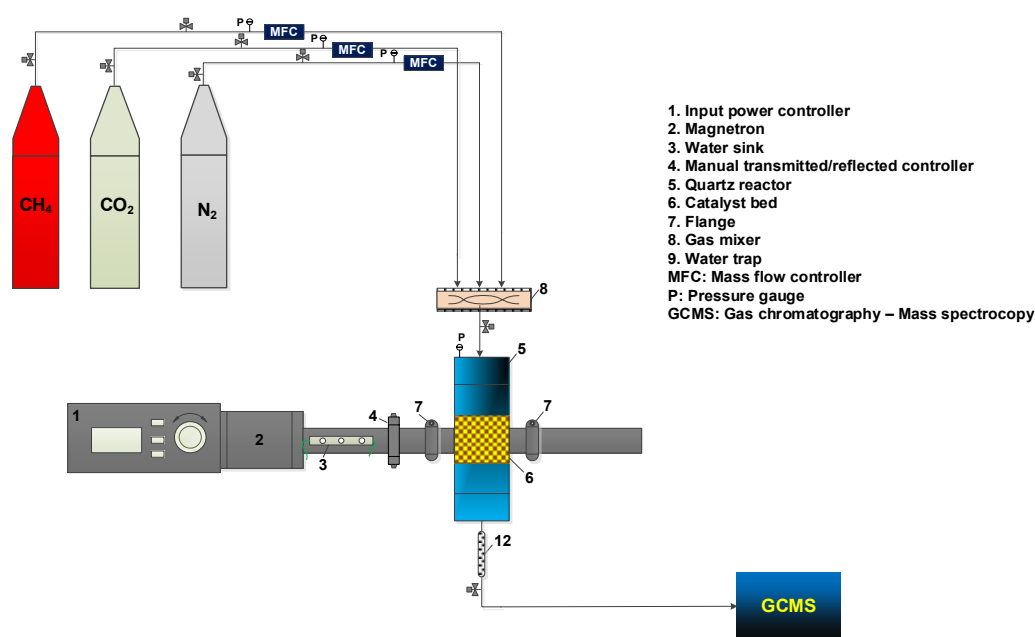


**Fig.S 1** Scheme of the catalytic DRM system heated by MW.

**Fig.S 1** shows the commercial MW reactor system for DRM (Alter, SM 1150T, Canada). The output power of the MW generator can be set flexibly between 0 and 3,000 *W* at a fixed frequency of 2.45 *GHz*. Two directional couplers were inserted into the microwave

guide system to monitor the forwarded/reflected MW power. The correct temperature measuring of the radiated materials is an important issue in microwave systems, due to non-uniform temperature distribution, the interaction between the metallic element and electromagnetic field and other challenges when using microwaves. In the literature, several works use the conventional thermocouples while other researchers utilize the infrared thermometers to record the catalyst bed temperature in MW irradiation system<sup>1-3</sup>. However, there are not accurate values because the complexity of MW behaviour with metallic catalysts inside the catalyst bed<sup>4-6</sup>. Thus, in this works, MW power was used as a process parameter to investigate its effects on catalytic activity and to repeat the experimental results.

The conversion of the reactants is defined by the following equations:

$$X_i = \frac{mole_{converted}^i}{mole_i^{in}} \cdot 100\% \quad (1)$$

Where,  $mole_{converted}^i$  is the molar conversion of gas,  $i$ , ( $mole \cdot min^{-1}$ );  $mole_i^{in}$  is the molar flowrate of gas,  $i$ , at the inlet ( $mole \cdot min^{-1}$ ).

H<sub>2</sub>, CO selectivity and syngas ratio can be calculated as:

$$S_{H_2} = \frac{mole_{H_2}}{2 \times mole_{CH_4}^{converted}} \cdot 100\% \quad (2)$$

$$S_{CO} = \frac{mole_{CO}}{mole_{CH_4}^{converted} + mole_{CO_2}^{converted}} \cdot 100\% \quad (3)$$

$$H_2 / CO = \frac{mole_{H_2}}{mole_{CO}} \quad (4)$$

Where,  $mole_{H_2}$  and  $mole_{CO}$ , are respectively the molar flowrate of  $H_2$  and  $CO$  produced ( $mole.min^{-1}$ );  $mole_{CH_4}^{converted}$  and  $mole_{CO_2}^{converted}$  are respectively the molar conversion of  $CH_4$  and  $CO_2$  ( $mole.min^{-1}$ ).

## Results and Discussion

### - Catalytic activity

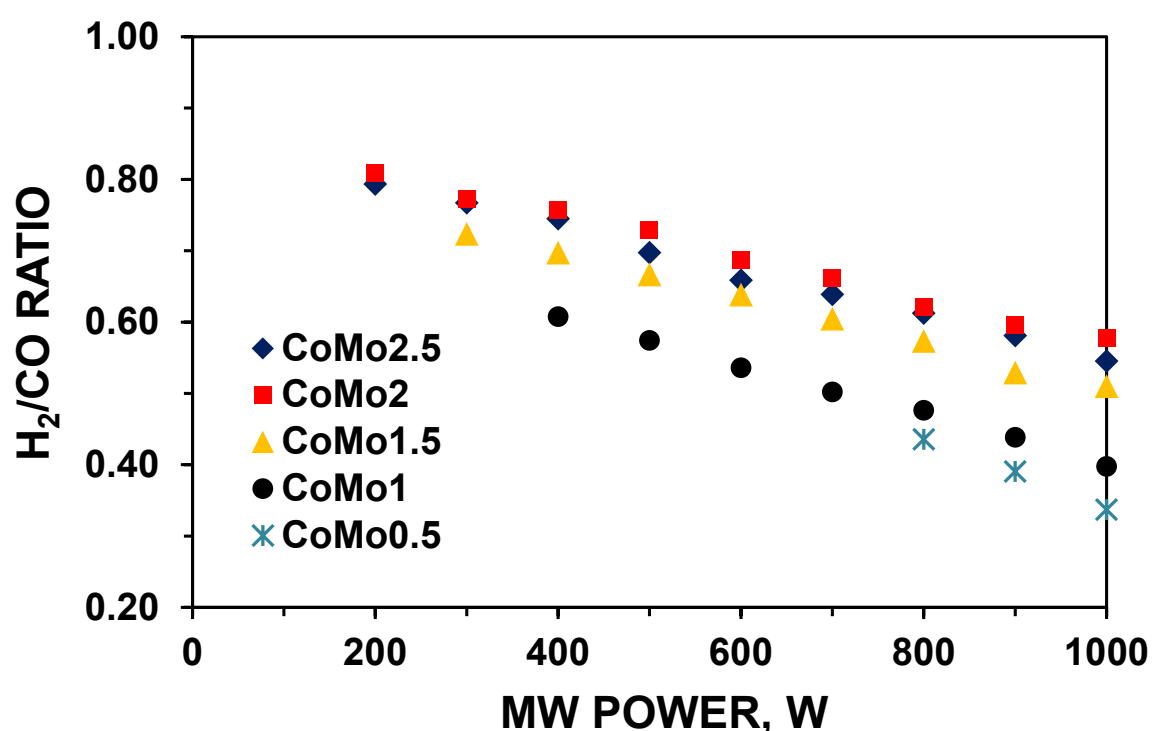


**Fig.S 2**  $H_2/CO$  ratio. [DRM reaction parameters:  $CH_4:CO_2=1$ ,  $VHSV = 10 L.g.h^{-1}$ ].

DRM under MW irradiated at 200 W over the CoMo2 catalyst can obtain  $H_2/CO$  ratio of 0.8 while that over the CoMo0.5 produces a syngas ratio of 0.43 at 500 W. However, the decrease in syngas ratio  $H_2/CO$  is observed when increasing MW power level (**Fig. S2**). This is due to the simultaneous occurrence of side reactions.

### Catalyst characterisation

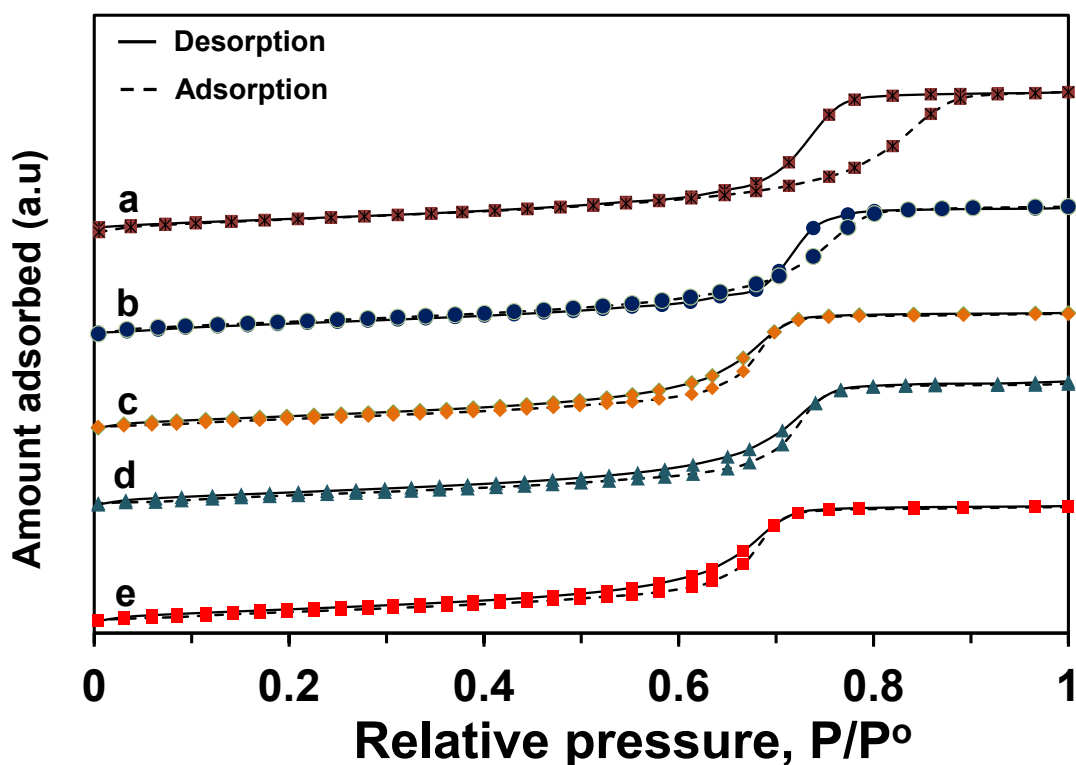


**Fig.S 3** N<sub>2</sub> adsorption/desorption isotherm curves of the reduced Co-Mo/Al<sub>2</sub>O<sub>3</sub> catalysts: (a) CoMo0.5; (b) CoMo1; (c) CoMo1.5; (d) CoMo2; (e) CoMo2.5. The N<sub>2</sub> adsorption/desorption isotherm curve of CoMo2 catalyst is represented here for comparison purpose.

The isotherm adsorption at low relative pressure ratio ( $P/P_o \leq 0.3$ ) of all reduced catalyst samples had lower nitrogen adsorption (lines close to X axis) than that of high relative pressure ratio, indicating a weak interaction between the nitrogen and catalysts. In contrast, at higher relative pressure, molecular clustering was followed by pore filling. Moreover, the cobalt loading presents the significant effects on the structure of catalysts. The hysteresis loops shifted from H<sub>2</sub> type (CoMo0.5, CoMo1) to H<sub>4</sub> type (CoMo1.5, CoMo2, CoMo2.5). According to the IUPAC recommendations, this result suggested an transformation from a structure with narrow necks and wide bodies (ink-bottle pores) (H<sub>2</sub>)

<sup>7</sup> to that of with aggregated of plate-like particles leading to slit-shaped pores and narrow slit-like pore, respectively <sup>8</sup>. The areas of the hysteresis loops becomes smaller and the isotherms of the reduced Co-Mo/Al<sub>2</sub>O<sub>3</sub> catalysts is shifted downward, which therefore suggest the decline in the BET surface areas.

Sample	BET (m <sup>2</sup> /g) <sup>a</sup>	Pore volume (cm <sup>3</sup> /g) <sup>b</sup>	Pore size (nm) <sup>c</sup>
Al <sub>2</sub> O <sub>3</sub> *	163	0.80	17
Mo/Al <sub>2</sub> O <sub>3</sub>	98.32	0.63	12.11
Co/Al <sub>2</sub> O <sub>3</sub>	94.22	0.71	14.33
CoMo0.5	79.28	0.42	10.12
CoMo1	65.53	0.40	9.23
CoMo1.5	60.57	0.37	7.55
CoMo2	58.75	0.28	7.43
CoMo2.5	49.23	0.21	5.28

**Table. S 2** BET and porosity of the fresh catalysts.

<sup>a</sup> Calculated by the BET equation

<sup>b</sup> Calculated by the BJH method using P/P<sub>0</sub> at 0.99

<sup>c</sup> Calculated by the BJH method using desorption branch

\*Acquired from Sasol Germany GmbH' specifications of supplied commercial Al<sub>2</sub>O<sub>3</sub>

The decrease in pore size and BET surface area was observed when increasing Co:Mo molar ratio from 0.5 to 2.5. This is due to the decrease of the concentration of alumina which is the major contributor to the high surface properties.

**Table. S 3** BET and porosity of the spent catalysts. [Reaction parameters: CH<sub>4</sub>:CO<sub>2</sub>=1, VHSV = 10 L.g.h<sup>-1</sup>].

Sample	BET (m <sup>2</sup> /g) <sup>a</sup>			Pore volume (cm <sup>3</sup> /g) <sup>b</sup>			Pore size (nm) <sup>c</sup>		
	200 W	500 W	1000 W	200 W	500 W	1000 W	200 W	500 W	1000 W
Mo/Al <sub>2</sub> O <sub>3</sub>	98.12	98.42	98.42	0.63	0.62	0.63	12.11	12.18	12.13
Co/Al <sub>2</sub> O <sub>3</sub>	94.62	94.02	94.02	0.71	0.74	0.71	14.33	14.41	14.35
CoMo0.5	73.28	64.22	52.31	0.53	0.49	0.39	10.12	9.89	7.14
CoMo1	60.53	57.56	51.37	0.38	0.34	0.30	9.23	9.00	6.55
CoMo1.5	56.57	52.23	50.28	0.35	0.32	0.26	7.55	7.11	4.23
CoMo2	53.75	51.23	46.15	0.32	0.30	0.24	7.43	6.82	3.12
CoMo2.5	46.23	44.23	34.43	0.20	0.18	0.11	5.28	4.15	1.08

<sup>a</sup> Calculated by the BET equation

<sup>b</sup> Calculated by the BJH method using P/P<sub>0</sub> at 0.99

<sup>c</sup> Calculated by the BJH method using desorption branch

\*Acquired from Sasol Company specifications of supplied commercial Al<sub>2</sub>O<sub>3</sub>

BET surface area as well as pore size of bimetallic catalysts was insignificantly altered at low irradiated MW power levels such as 200 W. These results also explain for the conservancy of catalytic activity over 16 TOS of CoMo2 catalyst at low MW powers. A considerable deterioration in textural properties of bimetallic catalysts are only observed at MW power of 1000 W. The reason for this is due to the sintering of metallic-based particles under high MW energy, which led to the formation of bigger particles occupying pore size and decrease surface area of catalysts.

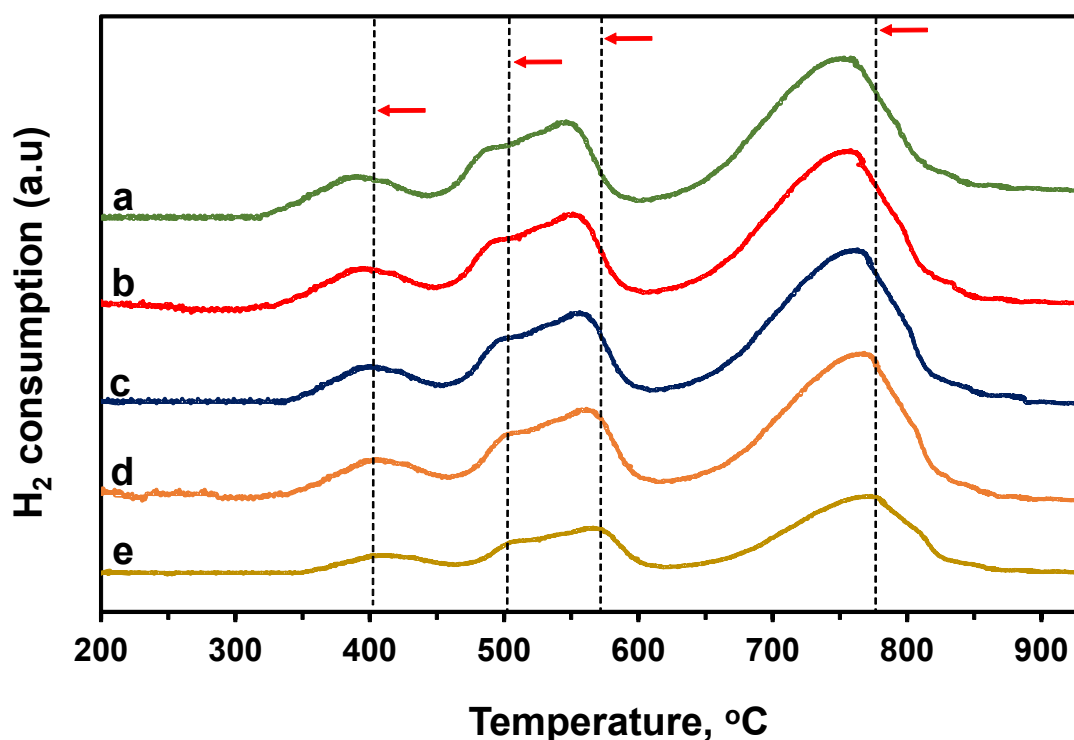


**Fig.S 4** TPR-H<sub>2</sub> profile of Co-Mo/Al<sub>2</sub>O<sub>3</sub> catalysts: (a) CoMo2.5; (b) CoMo2; (c) CoMo1.5; (d) CoMo1; (e) CoMo0.5 The TPR-H<sub>2</sub> profile of CoMo2 catalyst is represented here for comparison purpose.

In TPR-H<sub>2</sub> each peak corresponds to a different oxide and the amplitude of each peak is proportional to the reaction rate. The amount of H<sub>2</sub> uptake during the reduction was measured by a thermal conductivity detector (TCD), which was calibrated by the quantitative reduction of copper oxide to the metallic copper. As can be seen that by increasing Co/Mo from 0.5 to 2.5, the reduction temperature of bimetallic catalyst samples also shifted to lower values (**Fig.S 4**). Thus, in a mixture form, either cobalt or molybdenum weakens the interaction of each metallic component with Al<sub>2</sub>O<sub>3</sub> support improving the reducible ability of metallic-based particles in bimetallic catalyst samples.

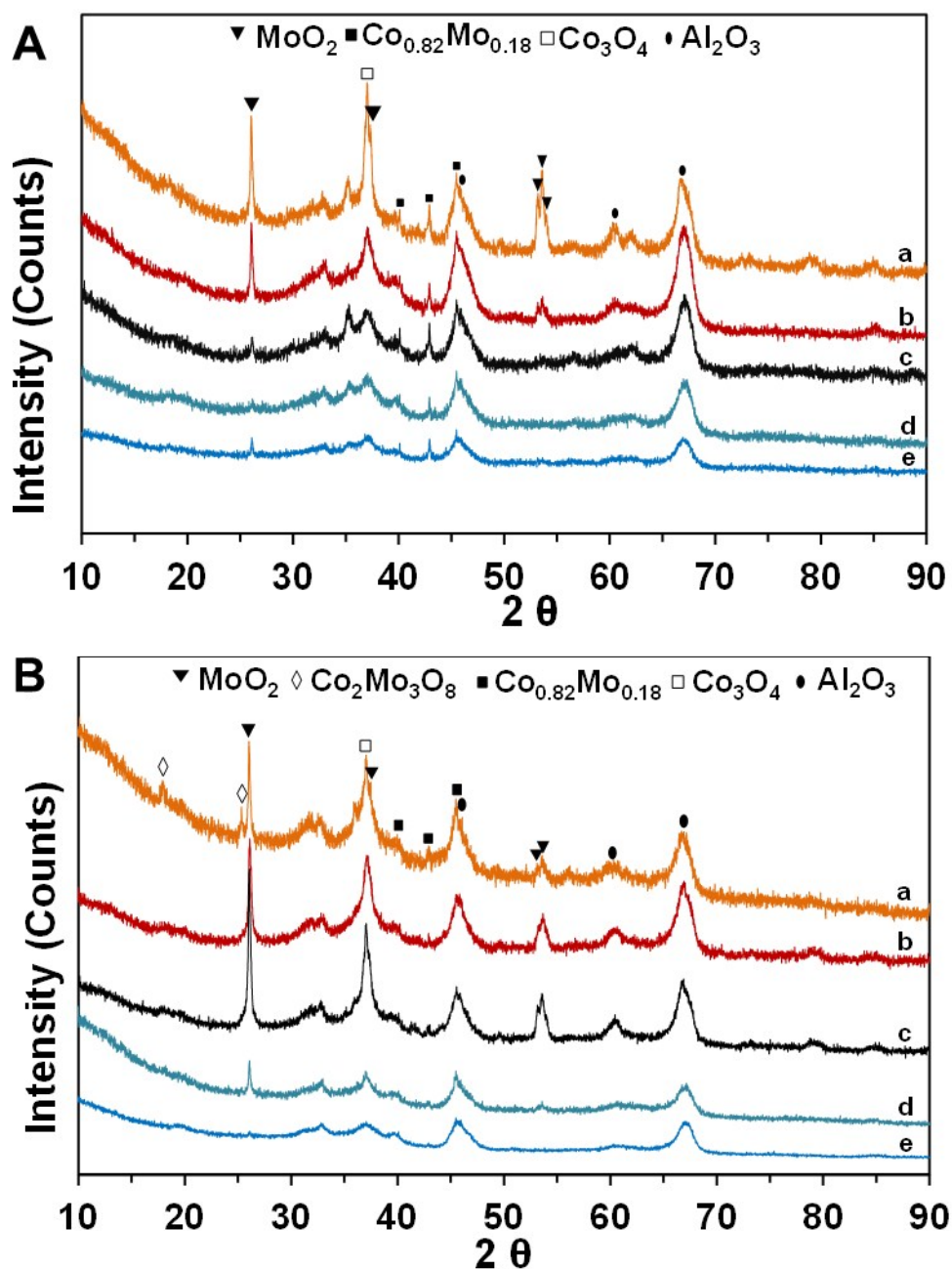


**Fig.S 5** XRD patterns of fresh (A) and spent (B) Co-Mo/ $\text{Al}_2\text{O}_3$  catalysts: (a) CoMo2.5; (b) CoMo2; (c) CoMo1.5; (d) CoMo1; (e) CoMo0.5. The XRD results of CoMo2 catalyst is represented here for comparison purpose. [Reaction parameters: MW power = 500 W,  $\text{CH}_4:\text{CO}_2=1$ , VHSV = 10 L.g.h<sup>-1</sup>].

The intensity of all diffraction peaks increased with the increment of Co/Mo molar ratio from 0.5 to 2.5. The presence of larger crystals in the catalyst structure presumably led to

the observed shifts of the hysteresis loops when increasing cobalt loading as shown in **Fig.S 3**<sup>9</sup>. After 16 h TOS of DRM reaction under MW irradiation, the patterns of MoO<sub>2</sub>, Co<sub>0.82</sub>Mo<sub>0.18</sub> and Co<sub>3</sub>O<sub>4</sub> are still detected from bimetallic catalyst (**Fig.S 5b**). This result reveals the stability of crystalline structure of bimetallic catalysts under redox environment of DRM reaction as well as MW irradiation leading to the enduring catalytic stability. However, the Co<sub>2</sub>Mo<sub>3</sub>O<sub>8</sub> phase is visibly identified at 17.87°, 25.29° (PDF 96-152-4069) from the spent CoMo2.5 catalyst. The Co<sub>2</sub>Mo<sub>3</sub>O<sub>8</sub> phase is an inactive phase which leads to the lower catalytic activity of CoMo2.5 catalyst than that of CoMo2.

In the present study, whole-pattern Rietveld refinement was performed on the XRD patterns to quantify the amounts of the different phases. The individual phase contribution used for Rietveld analysis are MoO<sub>2</sub> and Al<sub>2</sub>O<sub>3</sub>, Co<sub>3</sub>O<sub>4</sub> Co<sub>0.82</sub>Mo<sub>0.18</sub>. Moreover, the Rietveld refinement results (**Table. S 4**) also indicates the cell parameters of Co<sub>0.82</sub>Mo<sub>0.18</sub> alloy assigned to a space group symmetry of *P 63/m m c* with a hexagonal crystallography ( $a = 2.5582 \text{ \AA}$  and  $c = 4.2231 \text{ \AA}$ ,  $\alpha = \beta = 90^\circ$ ). The weight percentage of phases in a XRD tested sample (approx. 0.1 g) calculated from the refinement analysis was in a close agreement with the nominal loading which is 30 wt. % metallic component and 70 wt. % Al<sub>2</sub>O<sub>3</sub>.

**Table. S 4** The Rietveld refinement results.

Phase	Phase information			
	Quant. (%)	a (Å°)	b (Å°)	c (Å°)
MoO <sub>2</sub>	10.25	5.5343	4.8420	5.6080
Al <sub>2</sub> O <sub>3</sub>	68.60	3.9410	-	-
Co <sub>3</sub> O <sub>4</sub>	14.25	8.0972	-	-
Co <sub>0.82</sub> Mo <sub>0.18</sub>	6.90	2.5582	-	4.2231

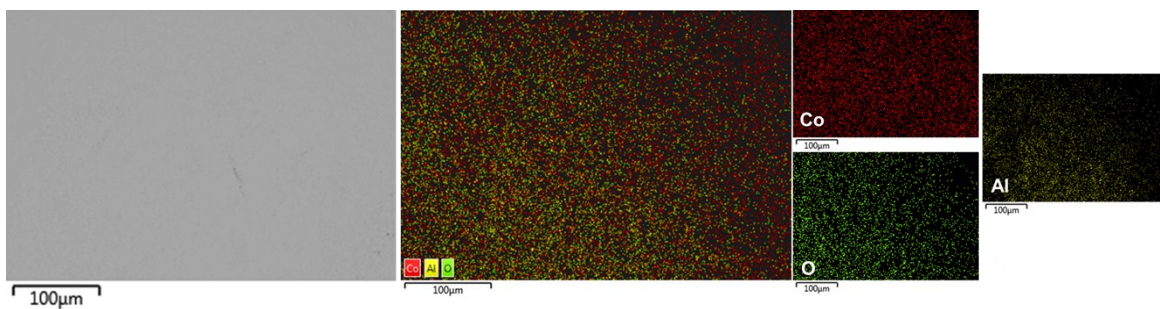


**Fig.S 6** FESEM images of fresh Co/Al<sub>2</sub>O<sub>3</sub> catalyst.

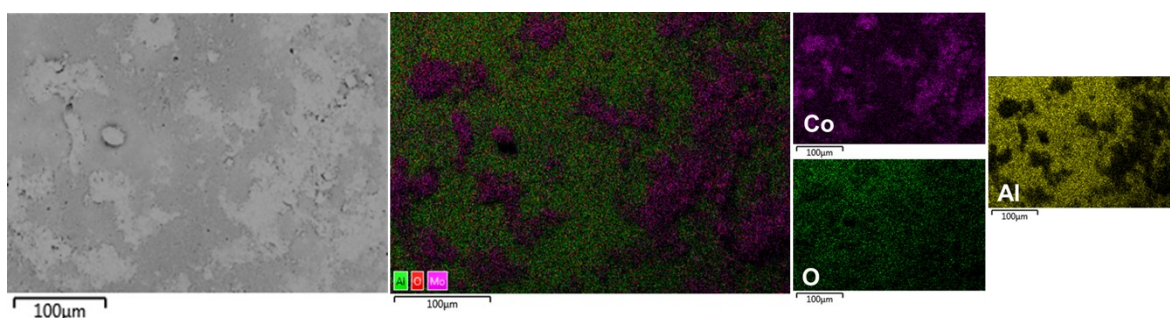


**Fig.S 7** FESEM images of fresh Mo/Al<sub>2</sub>O<sub>3</sub> catalyst.

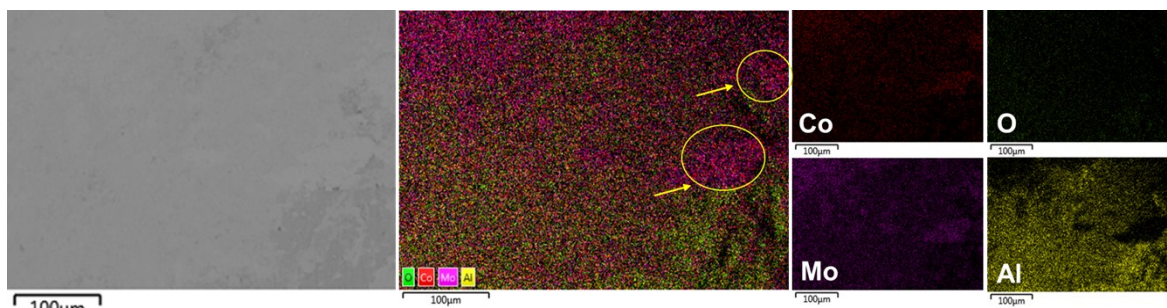


**Fig.S 8** FESEM images of fresh Co-Mo/Al<sub>2</sub>O<sub>3</sub> catalyst.

The well dispersion of metallic-based particles on the support was visibly indicated by FESEM-EDX results. As can be seen that Co-based particles are very well dispersed on the support surface of Co/Al<sub>2</sub>O<sub>3</sub> catalyst affirming its absence of diffraction peaks from the XRD pattern. In the meantime, the fresh CoMo<sub>2</sub> catalyst visibly displays locations in which contain a larger amount of Co and Mo atoms revealing the presence of bimetallic alloy.

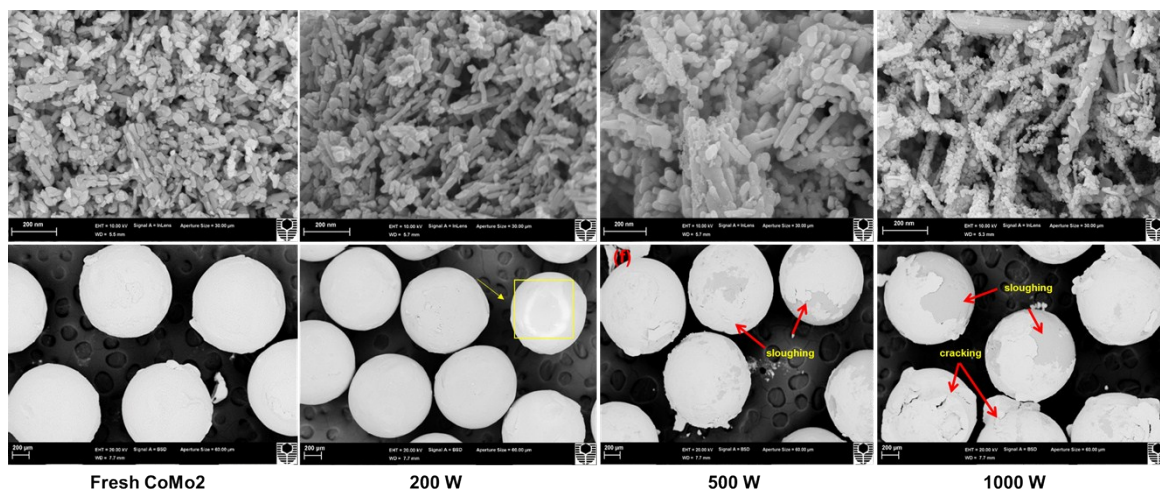


**Fig.S 9** FESEM images of fresh and spent CoMo<sub>2</sub> bimetallic catalysts at different magnifications. The results of CoMo<sub>2</sub> catalyst is represented here for comparison purpose.

Hence, the FESEM analysis at different magnifications and MW power levels for spent CoMo<sub>2</sub> catalysts was performed and the results (**Fig.S 9**) exhibit the sloughing and distortion on the bimetallic catalyst surface after 16 h on stream of DRM reaction under MW irradiation at 500 W. These deteriorations are particularly serious at higher MW power levels i.e., 1000 W. On the other hand, at a lower MW power of 200 W in which CoMo<sub>2</sub> catalyst can convert a relatively high reactant gas conversions (80 % CH<sub>4</sub> and 93 % CO<sub>2</sub>), there is not much difference between the fresh and spent catalyst samples morphology. Thus, the physical deterioration would be a principal reason leading to the above-observed decrease in catalytic activity at high MW power levels.

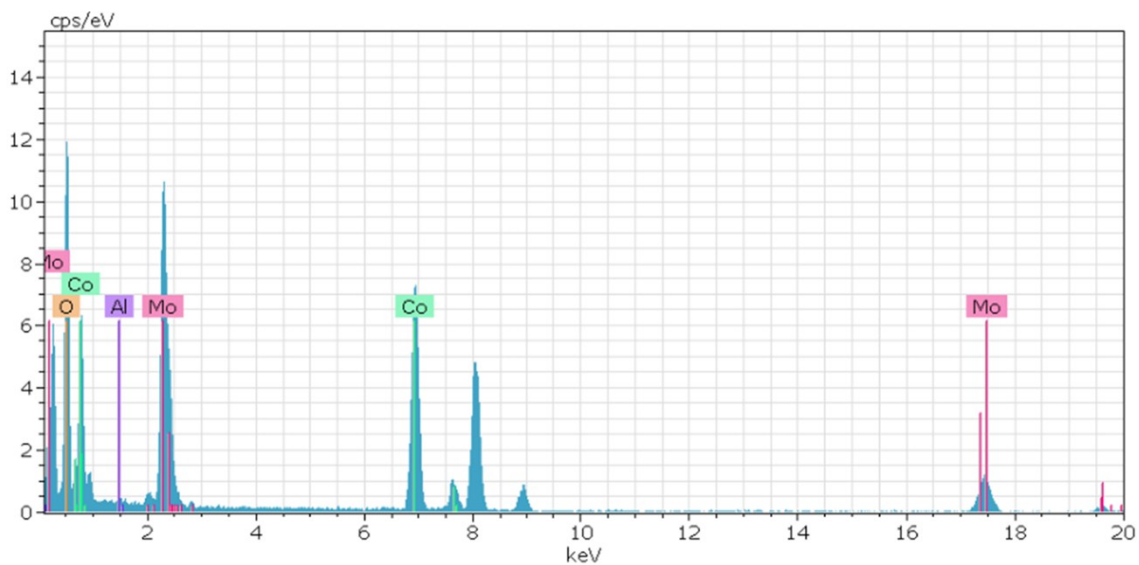


**Fig.S 10** STEM-EDX qualitative spectrum of fresh CoMo<sub>2</sub>.

In the mean times, the STEM-EDX qualitative spectrum of fresh CoMo<sub>2</sub> catalyst confirms all constitutive elements i.e., Co, Mo, O and Al. The unlabelled peaks are belong to the Cu-grid.

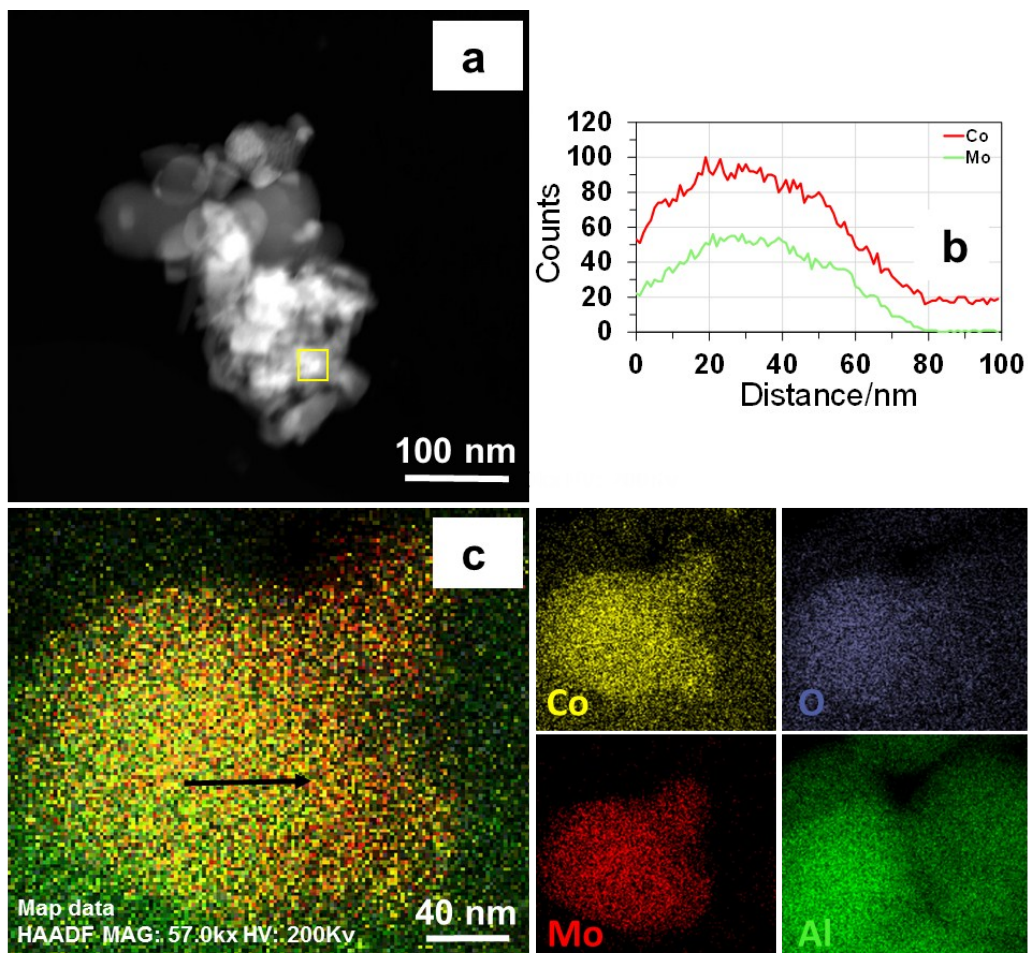


**Fig.S 11** STEM-HAADF (a), line-scanning signals (b), and STEM-EDX (c) of spent CoMo<sub>2</sub> catalyst. [Reaction parameters: 500 W, CH<sub>4</sub>:CO<sub>2</sub>=1, VHSV = 10 L.g.h<sup>-1</sup>].

As shown in for the line-scanning analysis (**Fig.S 11c**), the Co and Mo signals are visibly detected. The line-scanning analysis is well in accord with the nanoscale mapping results (**Fig.S 11b**), which also manifest that the Co and Mo components are overlaid on each other which elicits Co<sub>0.82</sub>Mo<sub>0.18</sub> bimetallic alloy.

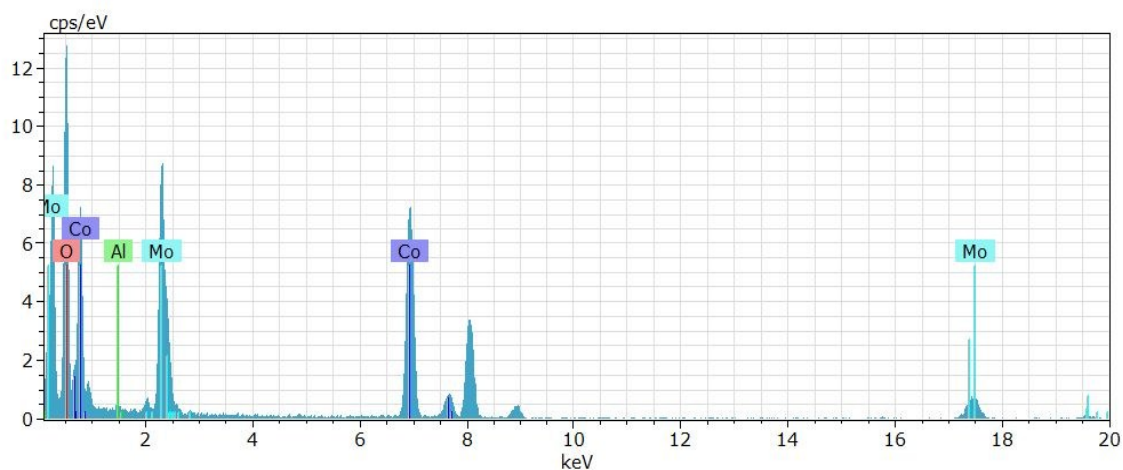


**Fig.S 12** STEM-EDX qualitative spectrum of fresh CoMo<sub>2</sub>.

Notably, carbon species such as graphite or carbon nanotube which are usually formed from DRM reaction <sup>10</sup>, could not be observed from the spent catalysts (**Fig.S 12**) echoing the physical stability of the bimetallic catalysts.

#### Notes and references

- 1 M. A. Herrero, J. M. Kremsner and C. O. Kappe, *The Journal of Organic Chemistry*, 2008, **73**, 36-47.
- 2 L. Li, X. Jiang, H. Wang, J. Wang, Z. Song, X. Zhao and C. Ma, *J. Anal. Appl. Pyrolysis*, 2017, **125**, 318-327.
- 3 L. Li, Z. Yang, J. Chen, X. Qin, X. Jiang, F. Wang, Z. Song and C. Ma, *Fuel*, 2018, **215**, 655-664.
- 4 T. Durka, T. Van Gerven and A. Stankiewicz, *Chem. Eng. Technol.*, 2009, **32**, 1301-1312.
- 5 N. Yoshikawa, *Journal of Microwave Power and Electromagnetic Energy*, 2010, **44**, 4-13.
- 6 L. S. Gangurde, G. S. J. Sturm, T. J. Devadiga, A. I. Stankiewicz and G. D. Stefanidis, *Ind. Eng. Chem. Res.*, 2017, **56**, 13379-13391.
- 7 F. He, J. Li, T. Li and G. Li, *Chem. Eng. J.*, 2014, **237**, 312-321.
- 8 Z. Cao, G. Liu, H. Zhan, C. Li, Y. You, C. Yang and H. Jiang, *Sci. Rep*, 2016, **6**, 36919.
- 9 C. Bueno-Ferrer, S. Parres-Esclapez, D. Lozano-Castelló and A. Bueno-López, *Journal of Rare Earths*, 2010, **28**, 647-653.
- 10 A. V. P. Lino, E. M. Assaf and J. M. Assaf, *Catal. Lett.*, 2018, **148**, 979-991.